High Yield Events of Molecular Emission Induced by Kiloelectronvolt Particle Bombardment

A. Delcorte and B. J. Garrison*

Department of Chemistry, The Pennsylvania State University, 152 Davey Laboratory, University Park, Pennsylvania 16802

Received: April 10, 2000

In an effort to improve our understanding of large molecule emission in organic SIMS, the sub-kiloelectronvolt and kiloelectronvolt Ar atom-induced sputtering of polystyrene tetramers adsorbed on Ag{111} is modeled using classical molecular dynamics. Above 1 keV, in addition to trajectories consisting of successive collisions between individual atoms, we observe a significant number of high action trajectories where several hundreds of substrate atoms are moving simultaneously. These events can generate unusually high emission yields of substrate atoms, clusters, and polystyrene molecules. Because the probability of high yield events strongly depends on the primary particle energy, representative sets of trajectories are calculated at 150 eV, 500 eV, 1500 eV, and 5 keV. These simulations indicate four main scenarios of action and sputtering. Plots of the energetic parts of the cascade ("collision trees") show that high sputtering yields occur when most of the primary particle energy is quickly dissipated among silver atoms belonging to the top silver layers. In addition, it is shown that high emission events influence not only the yield but also the kinetic energy distributions of ejected polystyrene molecules. Finally, we discuss the relevance of these high yield mechanisms for the ejection of organic species with a mass of several kilodaltons such as biomolecules and synthetic polymers. Our results show that trajectories falling in the "high yield" category are also capable of desorbing large intact molecules of ∼2000 Da.

1. Introduction

The analysis of large organic species, including biomolecules and synthetic polymers, constitutes an important field of applications in mass spectrometry. In this domain, the performance of a technique depends on its ability to produce and detect high mass ions. Several techniques are appropriate for the analysis of nonvolatile molecules with a mass beyond one kDa. Historically, the technique that opened the door to biological mass spectrometry is fast atom bombardment mass spectrometry (FABMS), the sister of static secondary ion mass spectrometry (SIMS), introduced by Barber and co-workers in 1981.[1] FABMS evolved from SIMS[2] by incorporating a liquid matrix instead of using solid samples and by using a primary beam of neutral atoms instead of ions. Since then, SIMS has also been significantly developed and the analysis of molecules up to 10 kDa is now achievable, owing to the combined use of energetic heavy monatomic (Cs^+, In^+) or polyatomic (SF_5^+) primary ions, time-of-flight (TOF) spectrometers, and new sample preparation methods, e.g., ionic salts,[3] transition metal substrates,[4] particles or overlayers[5] as well as hydrogen-donor matrices.[6] In the past decade, the accessible mass range has been tremendously expanded by two new spectrometric techniques using Matrix-Assisted Laser Desorption Ionization (MALDI)[7] and Electrospray Ionization (ESI)[8] as ion sources. With these methods, the desorption/ionization and the structural analysis of biopolymers such as proteins or carbohydrates with a molecular weight of more than 100 kDa is routinely performed. Recently, oligomers of mouse IgG monoclonal antibody, heavier than 1 MDa, have been successfully emitted and detected with MALDI MS,[9,10] as well as a 100 MDa DNA molecule using an ESI source coupled to a Fourier Transform-Ion Cyclotron Resonance (FT-ICR) mass spectrometer.[11]

Although the mass range of TOF−SIMS is more limited, it has a few advantages over MALDI and ESI that are critical for certain applications. First, TOF−SIMS is remarkably versatile and can analyze almost any kind of solid surface.[12] In comparison with ESI and MALDI, SIMS does not usually need complex sample preparation methods involving dissolution in a well-chosen solvent or in a complex acidic matrix that might be harmful for the analyte. Consequently, it allows experimentalists to analyze samples as received and to address issues related to real or industrial processes in a direct way. TOF−SIMS is also very sensitive, owing to the parallel detection of all the sputtered ions by TOF spectrometers, and it has impressive chemical imaging capabilities, because of the easy focusing of primary ion beams that provides submicrometer lateral resolution.[13] In the arena of biology, it has proved to be useful for the analysis of frozen cells, tissues, and membranes and for the characterization of tumors in medical studies. In the chemical and biochemical fields, it is a powerful means to identify complex organic molecules and mixed systems containing several different molecules.[14] Therefore, the Holy Grail for SIMS users would be to extend the mass range of the technique while keeping its other advantages, e.g. its unique capability to analyze real-world samples. In the past few years, forays have been done in several directions to overcome the mass range limitation, but the fundamental studies aimed at identifying the causes of this problem are sparse. If one excludes detection-related issues, the factors that prevent SIMS analysis of large molecules may be related either to the difficulty to desorb large species or to the lack of efficient ionization mechanisms for the desorbed species.

The successful ionization of molecules larger than 100 kDa in MALDI MS and ESI MS indicates that the physical limit in SIMS mainly resides in the desorption step of the process. In this respect, the comparison between SIMS and laser ablation

* Phone: 1-(814)-863-2103. Fax: 1-(814)-863-5319. E-mail: bjg@psu.edu.

10.1021/jp001374h CCC: $19.00
Published on Web 06/29/2000

is illuminating. In SIMS, the primary particle usually induces the development of a collision cascade in the top layers of the sample. A part of the primary particle energy can be reflected toward the surface through some subcascades, causing the ejection of secondary species from localized spots on the surface. In laser ablation, the fast energy transfer to a relatively large volume of material causes collective motion and expansion of this volume toward the vacuum.[15] In the particular case of MALDI, this expansion entrains large analyte molecules and clusters within the plume of matrix molecules, without extensive fragmentation or large internal energy excess. Therefore, it appears that large-scale collective motions might be the key to desorption of heavy intact molecules from solid surfaces. Although large-scale events as those observed in laser ablation are probably impossible to obtain with kiloelectronvolt primary ions, there exists in sputtering a class of events which bear some resemblance to ablation processes. In the literature, they have been referred to as *spikes*[16−19] or *megaevents*,[20,21] as opposed to linear collision cascades.

Experimentally, the existence of these peculiar events is difficult to demonstrate, although they are strongly suggested by very high sputtering yields as those observed, for example, when a gold target is bombarded by gold atoms and clusters.[22] In turn, the influence of experimental parameters such as the primary ion nature, energy and incidence angle or the nature of the sample on such events can hardly be tested without the help of a reliable theoretical model. Such a model can be validated by comparison of the predictions to experimental yields, kinetic energy and angular distributions of sputtered molecules.

Besides Sigmund's sputtering theory,[16,17] the idea of correlated motion of the target atoms has been developed in analytical models of kiloelectronvolt and megaelectronvolt particle bombardment of solids to explain the emission of large material clusters and biomolecules that are unlikely to arise from direct electronic excitation (megaelectronvolt) or from binary collisions between atoms (kiloelectronvolt). In this context, large polyatomic species are thought to emerge from regions where many atoms are moving with nearly parallel and equal momentum, as a result of the fast conversion of electronic/collisional excitation into large scale correlated motion. Collective mechanisms have been described with different premises in the gasflow,[23,24] shock wave[25−29] and pressure pulse[30] models. These models were invoked in the case of kiloelectronvolt particle bombardment of metals,[31−33] biomolecules[34,35] and condensed amorphous rare gases.[36] Regarding the ejection of metal clusters and organic molecules, however, the above models have not been tested under sufficiently stringent conditions to be definitely validated by experimental results, much less to be used in a predictive way.

In the kiloelectronvolt primary energy range, classical molecular dynamics simulations performed with monocrystalline metal samples indicate that high action (or high energy density[37]) events are related to particular trajectories in which the energy of the primary projectile is quickly distributed among the atoms belonging to the surface layers of the sample. In turn, many atoms are simultaneously set in motion in the subsurface region, leading to high ejection yields of metal atoms and clusters. Such high action events have been observed by several authors[19−21,38,39] and, in particular, they have been pointed out by Betz and coworkers to explain the emission of large clusters under kiloelectronvolt particle bombardment.[39−41] They are usually associated with significant damage in the sample.[20,42]

Although the picture is far from complete, the existing body of theoretical studies indicates that the primary particle nature, energy and incidence angle should influence the probability of high action events. Large-scale simultaneous motion in the sample surface is generally thought to be favored by high mass or high energy primary particles (PP), by off-normal incidence angles and by polyatomic projectiles. The influence of the sample nature and composition is probably more complex, as is elegantly indicated by reports of MD simulations involving polyatomic projectiles along with various sample substrates.[43,44] Unfortunately, detailed studies involving large organic molecules, bulk organic materials or molecular solids are not yet available. Recently, a short report provided interesting indications about damage and sputtering in a polyethylene sample bombarded by kiloelectronvolt argon atoms.[45,46] Although van der Waals interactions were not taken into account, this report indicates that the late ejection of large fragments might be induced by collective/vibrational motion. Again, MD studies appear to be the only method able to deal with these organic matrices in the near future.

In a previous article, the ejection of polystyrene (PS) tetramers (474 amu) adsorbed on silver under 500 eV Ar atom bombardment has been modeled using MD simulations.[47] This study helped us to gain insights into the emission and fragmentation mechanisms of such relatively large molecules. Even with 500 eV projectiles, cooperative uplifting events where the organic molecule is gently pushed upward by several substrate atoms occur and they appear as the more efficient way to eject molecules with a low internal/kinetic energy ratio, i.e., molecules that would reach the detector intact in the experiments. Nevertheless, the observed cooperative motions were restricted in size and the affected volume in the surface region did not exceed the size of the polystyrene tetramer. In turn, our guess was that the efficient ejection of significantly larger molecules (several thousands of amu) as observed in the experiments would require, or at least would be strongly favored, by larger scale events. Our preliminary simulations at 5 keV indicated the presence of these more dramatic events. The occasional development of high action and high yield events for particular impact points is indeed the major difference between the 5 keV and the 500 eV primary beam excitations. At the time, the small number of 5 keV trajectories did not allow us to present a comprehensive view of such events, of their dependence on the primary particle kinetic energy and of their influence on the ejected molecule properties. This is the main objective of the present paper.

The discussion is organized in three sections. First, we show the evolution of the yields of sputtered atoms, fragments and entire molecules as a function of the PP energy. These results help us to introduce a clear definition of high action and high yield events. In the second section, our definition is used to identify four major mechanistic scenarios and to find a few representative trajectories providing a good illustration of these scenarios. In the third section, the influence of high yield events on the properties of the ejected molecules is demonstrated. Finally, we propose arguments that suggest the particular relevance of these events for the emission of larger organic molecules.

2. Method

The Ar bombardment of *sec*-butyl terminated polystyrene tetramers (Figure 1) adsorbed on a Ag(111) surface is modeled using molecular dynamics (MD) computer simulations. The MD scheme has been described in extensive detail elsewhere.[20,48−51] Briefly, it consists of integrating Hamilton's equations of motion over some time interval to determine the position and velocity

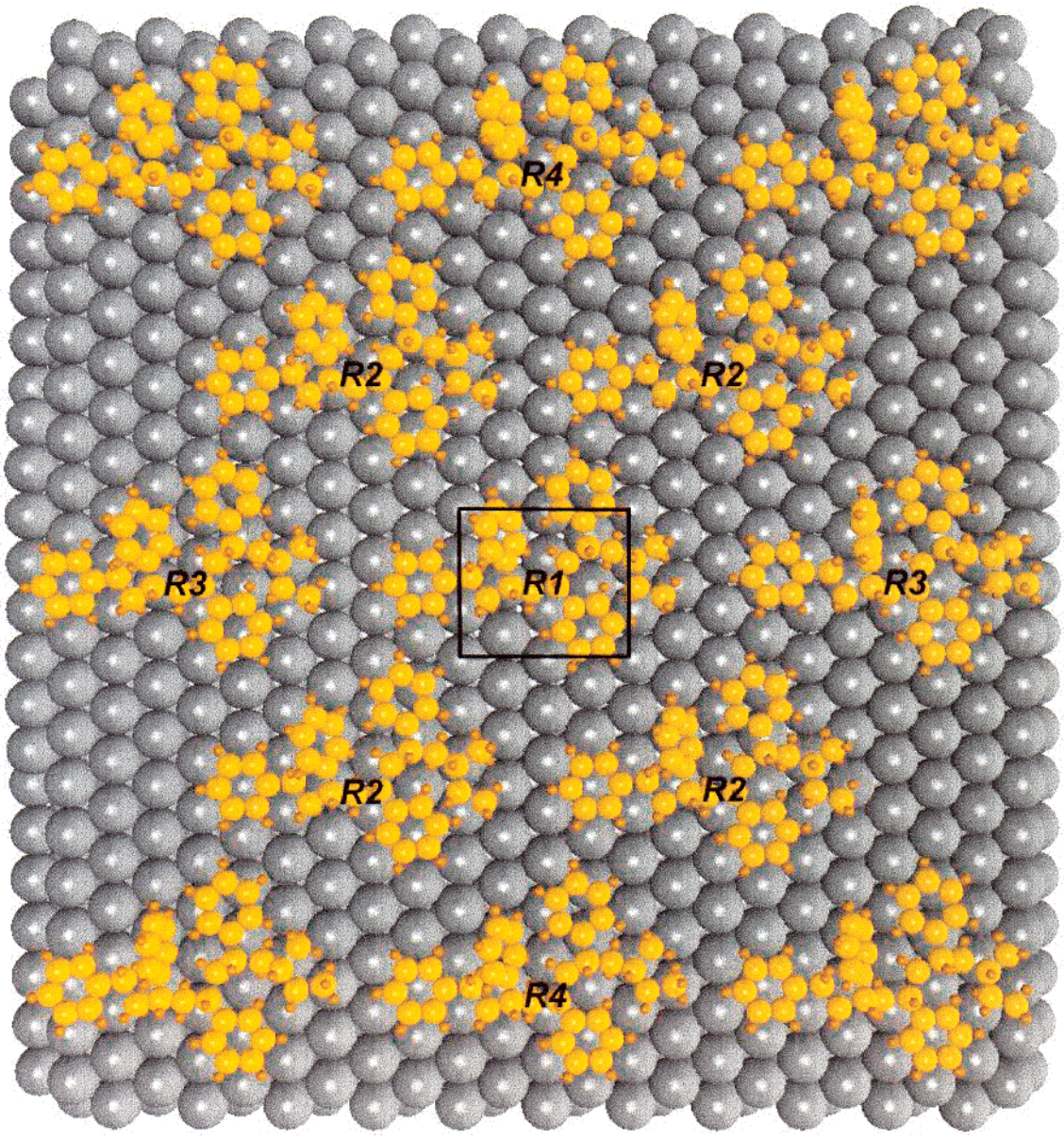

Figure 1. Surface configuration of the samples used for 1.5 and 5 keV Ar atom bombardment. Silver atoms are represented by large gray spheres, carbon, and hydrogen by golden spheres. The bombarded area is indicated by a rectangle. The labels refer to the different peaks in Figure 4a. See text in section 3.1 for details.

TABLE 1: Properties of the Simulation Cells and Numbers of Trajectories Calculated in the Different Bombardment Conditions

PP energy	no. of Ag layers	no. of Ag atoms per layer	no. of PS molecules	no. of trajectories
150	7	156	5	1000
500	9	156	5	4000
1500	10	528	13	1000
5000	12	528	13	500

of each particle as a function of time. The energy and forces in the system are described by many-body interaction potentials. Experimentally observable properties are calculated from the final positions, velocities, and masses of all the ejected species. Mechanistic information is obtained by monitoring the time evolution of relevant collisional events.

The sample characteristics and the number of trajectories corresponding to the different bombardment conditions are summarized in Table 1. In the model, the silver substrate is approximated by a finite microcrystallite containing 7−12 layers of Ag atoms, depending on the PP energy. Several (5−13) organic molecules are placed on the Ag{111} surface as shown in ref 47 for the 150 and 500 eV bombardment conditions and in Figure 1 for the 1.5 and 5 keV bombardment conditions. A small number of 5 keV trajectories are also calculated with a different sample in which the 12 molecules surrounding the aimed PS tetramer in Figure 1 are replaced by two PS hexadecamers (16 styrene repeat units). Each system is quenched to a minimum energy configuration prior to Ar atom impact. Primary Ar atoms are directed along the surface normal. Except for the system including PS hexadecamers, a representative set of Ar aiming points or trajectories directed within the impact area (rectangle in Figure 1) were calculated. For the impact area, we define a central zone that includes both molecule and bare substrate, as was explained in ref 47.

Each trajectory is initiated using a fresh undamaged sample. The criterion for terminating the trajectory is that the total energy of any atom is too low to induce ejection. The termination times range from 0.5 to 6 ps, depending on the impact point of the primary particle and the manner in which the energy distributes

within the solid. Open boundary conditions are used for the system.[20,50] That is, energetic particles that reach the sides or bottom of the computational cell are allowed to exit, taking their energy with them. In all the considered systems, the mass of hydrogen was taken to be that of tritium (3 amu) to increase computational efficiency.[52]

The blend of empirical pairwise and many-body potential energy functions used to represent the forces among the various atoms has been described in detail elsewhere.[52] Briefly, we use a purely repulsive Moliere potential to describe all interactions between the Ar and other atoms. This assumption is based on the fact that the Ar atom primarily imparts energy and momentum to the system and does not play a direct role in the chemistry of the bombardment process. For the remainder of the system, both the repulsive and attractive interactions are evaluated using many-body and pairwise potential functions. The Ag−Ag interactions are described by the molecular dynamics/Monte Carlo corrected effective medium (MD/MC−CEM) potential function for fcc metals.[53−55] The hydrocarbon interactions are described by the Brenner potential function.[56,57] This potential was fit to the energetics and structures of small hydrocarbon molecules, including radicals as well as graphite and diamond lattices. It allows for chemical reaction and accompanying changes in atomic hybridization during the course of a reaction. It is important to note that this hydrocarbon potential is confined only to short-range interactions of nearest neighbors and that long-range van der Waals type interactions are not included. As described in ref 58 a Moliere function is attached to the repulsive wall of the Brenner potential in order to handle high-energy collisions. The interactions for Ag−C and Ag−H are described by pairwise additive, Lennard-Jones potential functions. The Lennard-Jones parameters are chosen to obtain a reasonable binding energy for benzene molecules adsorbed on the silver surface.[52] The Ag−C and Ag−H equilibrium distances of 2.3 Å were taken from an estimate for the height of benzene molecules above the Ag{111} surface,[59,60] and the energy well depth for the Ag−C and Ag−H interaction are, respectively, equal to 0.05 and 0.0083 eV. The binding energy of PS molecules is obtained by subtracting the sum of the total energy of the relaxed silver crystal and PS molecules (in vacuo) from the total energy of the relaxed crystal with adsorbed molecules. With the above parameters, the binding energy of one PS tetramer to the silver substrate is ∼2.3 eV, and that of one PS hexadecamer is ∼7.2 eV.

At the end of each simulation, the atoms, clusters and molecules which have velocities directed away from the surface and are at a height of 6 Å above the original sample are regarded as ejected. For identifying clusters, pairs of atoms are checked to see if there is an attractive interaction between them, in which case they are considered linked.[48,61,62] A network of linked pairs is constructed and the total internal energy of the group is evaluated. If the total internal energy is less than zero, then the group of atoms is considered to be an ejected molecule. This procedure, of course, overestimates the number of bound ejected molecules as some of these aggregates may have sufficient internal energy to decay unimolecularly during the flight to the detector.[62] The yields described in Figures 3−6 correspond to molecules and fragments identified using this procedure (nascent species). On the other hand, we apply the correction protocol of ref 47 to obtain the kinetic energy distributions of stable molecules shown in Figure 12.

3. Results

High sputtering yield events are the focus of this article. Nevertheless, before going into mechanistic details, it is essential to be armed with a sensible and practical definition of the concepts of high action and high sputtering yield. In section 3.1, we define these two concepts on the basis of the sputtering yields and the number of displaced silver atoms provided by the MD simulation. The clear dependence of such numbers on the primary particle energy will be demonstrated. With the help of tractable definitions, we are able to isolate four main action and ejection scenarios. They are illustrated and explained in section 3.2, using a few illuminating examples of trajectories. Finally, section 3.3 addresses the influence of the high yield events on the properties of the ejected molecules.

A particularly interesting trajectory, observed under 5 keV Ar bombardment and involving high action in the substrate and high sputtering yield of silver atoms and PS molecules, will be used as a benchmark for the reader along the discussion. The action occurring in this trajectory is illustrated in Figure 2a-c by three snapshots of the MD simulation and in Figure 2d by a plot of the energetic part of the collision cascades (collision or 'lean-on' tree[63]). The meaning of the collision tree displayed in Figure 2d is explained at length in section 3.2. The initial configuration of the sample is shown in Figure 1. After 100 fs, the silver crystal seems almost intact, except for a few relatively fast silver atoms that are ejected from the top layer along with two hydrogen atoms (Figure 2a). At 300 fs, the effect of the massive energy flow into the crystal begins to be obvious, as witnessed by the large number of silver atoms protruding on the surface and on one corner of the crystal (Figure 2b). PS molecules are slowly lifted up by the upward moving silver atoms. After 1 ps, almost all the silver atoms are in motion. A disordered volume including several hundreds of atoms is formed in the crystal surface. Most of the moving Ag atoms are slow and unable to escape the potential well of the crystal, but a significant number receive a sufficient amount of energy to leave the surface. It is interesting to note that, at this time, often described as the onset of the spike regime,[19,21,41] silver atoms depart the crystal in aggregates that will form separate clusters out of the potential well of the surface. The PS molecules leave the surface within the flux of silver atoms and clusters.

In summary, the main features of this trajectory include the simultaneous motion of a very large number of substrate atoms (high action) and the massive ejection of silver atoms, clusters and polystyrene molecules (high sputtering yield). In the following section, high action and high yield events such as the one described above will be defined more precisely.

3.1. High Sputtering Yield and High Action Trajectories.

(a) Yield of Sputtered Species and Dependence on the Primary Particle Energy. To introduce the definition of high yield trajectories, it is useful to consider the evolution of the secondary particle yields when a relevant property of the primary particle varies. On the grounds of a preliminary study, the kinetic energy of the PP appears as a sensible parameter with respect to the onset of high yield events. The variation of the mass or the nature of the PP (e.g., polyatomic vs monatomic projectile) would probably be as relevant and informative, but an analysis based on these variables would imply the simultaneous modification of several physical parameters at the time. Indeed, the mass of an atom cannot be isolated from its other characteristics, and the comparison with polyatomic projectiles would involve questions concerning group and geometrical effects. Therefore, the PP energy appears to be the variable of choice to explore situations in which high yield events are absent as well as conditions in which they occur.

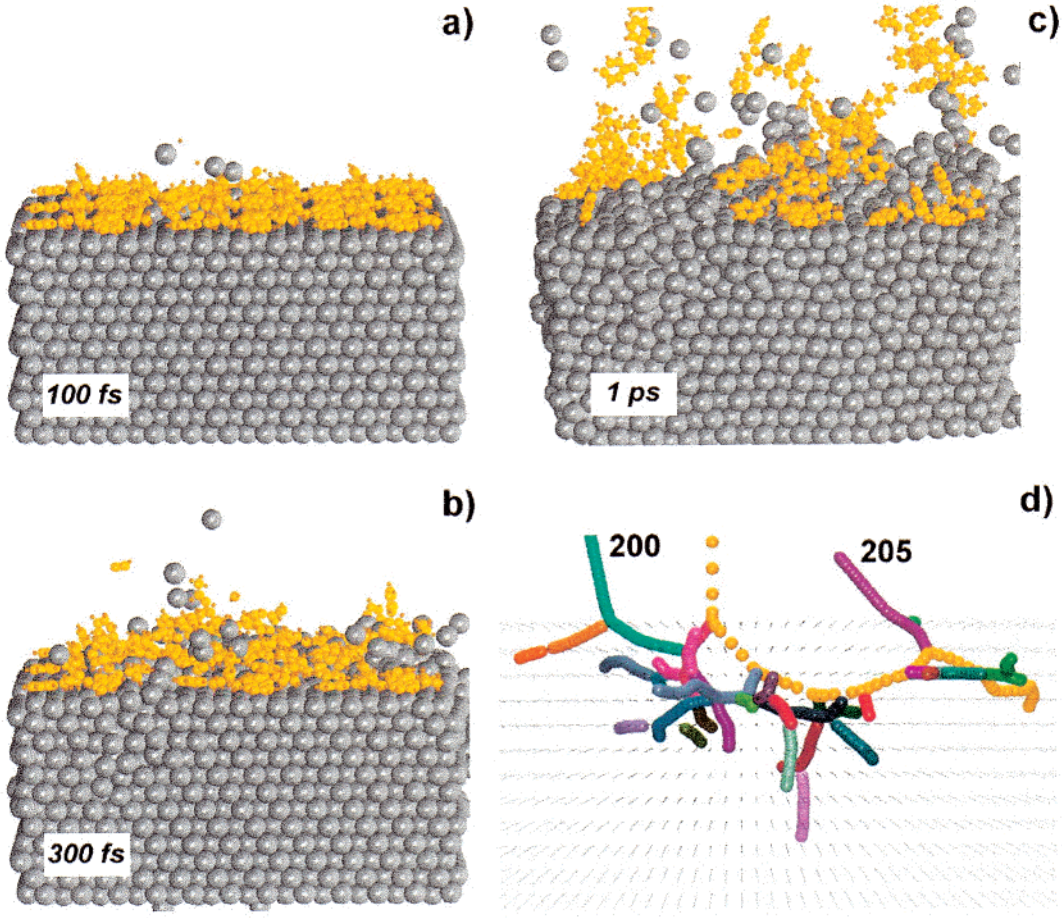

Figure 2. Time evolution of a high yield trajectory under 5 keV Ar bombardment: (a) 100 fs; (b) 300 fs; (c) 1000 fs. (d) Collision tree showing the high energy part of the cascades after 100 fs for the same trajectory (E). The incident particle is represented by yellow spheres. See text for details.

The information concerning the evolution of the yields of atoms, molecules and fragments is gathered in Figure 3. The influence of PP energy on the yield of monatomic sputtered species, Ag, C and H atoms, is displayed in Figure 3a. The Ag atom yield increases monotonically by more than 1 order of magnitude between 150 eV and 5 keV, as might be expected considering the increase of the nuclear stopping power in this energy range. In contrast, the emission yields of C and H atoms undergo a maximum around 1 keV and decrease afterward.

The yield variation of organic fragments and parent molecules is plotted in Figure 3b. The data indicate very different behaviors depending on the considered fragments. The sustained increase of the entire molecule yield is very well correlated to the yield increase of the substrate silver atoms shown in Figure 3a. In sharp contrast, the yield variation of fragments is much less dramatic. While the deprotonated molecules [M−H] still exhibit a marked increase in yield between 150 eV and 5 keV, other characteristic fragments (C_6H_5, $C_{12}H_{17}$) show almost no variation in this energy range. The evolution of smaller fragments such as acetylene molecules reflects the behavior of C and H atoms.

The decrease of the C and H atom yields beyond 1 keV might be partly related to the nature of the sample, where the organic molecules are arranged as a thin overlayer on top of the bulk Ag crystal. In this configuration, the energy deposited in the silver crystal is expected to increase steadily, while the energy deposited in the organic overlayer might saturate or decrease because most of the PP energy preferentially flows into the bulk beyond a certain point.

The microscopic view of the emission process provided by the MD simulations suggests a complementary explanation for the behavior of fragment and parent molecule yields. It has been shown in ref 47 that parent molecules are mostly ejected as a result of collision cascades developing in the silver substrate, which eventually lift them up when recoil Ag atoms reach the sample surface. Therefore, the good correlation between Ag atom and PS molecule yields could be expected. Moreover, the MD simulations show that the average ejection area expands with increasing energy for silver atoms, clusters and PS molecules. The variation of ejection area with PP energy is best shown in Figure 4. In this figure, the yields of ejected fragments or molecules are plotted as a function of the distance between the primary particle impact and the center of mass of the ejected species prior to emission. The curves corresponding to the ejection area of entire molecules are shown in Figure 4a. Only 500 eV and 5 keV distributions are presented for the sake of clarity, but the evolution is gradual between 150 eV and 5 keV. First, the 5 keV distribution exhibits a peak pattern that is less visible in the 500 eV distribution. This pattern is related to the arrangement of the PS molecules on the silver surface with respect to the bombarded area. A simple analysis of the peak distances in relation with the top view of the simulation cell in Figure 1 indicates which molecules contribute to the different peaks. The peaks and corresponding molecules are marked as R1, R2, R3 and R4 in Figure 1 and Figure 4a, in reference to the successive "rings" around the impact zone to which the molecules initially belong.[44] Second, the 5 keV distribution is much broader than the 500 eV distribution. Under 5 keV

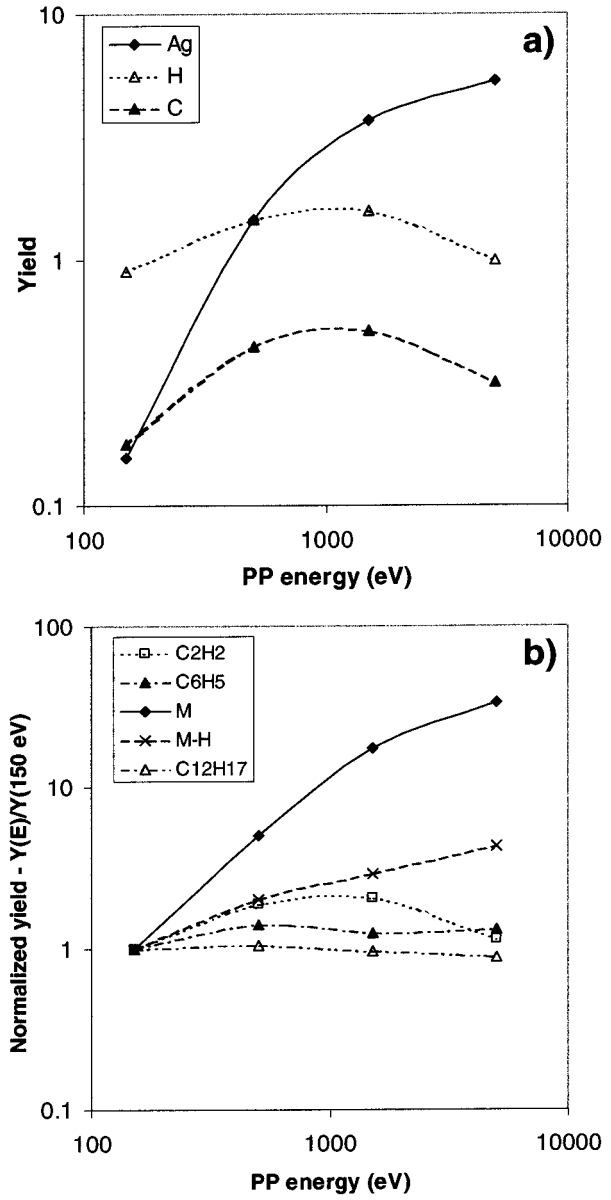

Figure 3. Dependence of the sputtered particle yields on the primary particle energy for (a) monatomic species and (b) polyatomic species.

bombardment, PS molecules originally lying more than 25 Å away from the impact point can be ejected. On the other hand, the 500 eV distribution tail quickly drops to zero within a radius of 15 Å around the impact point. In other words, the number of candidates for ejection increases with PP energy, accounting for the observed yield increase. In contrast, fragments are formed by the interaction between the incident particle and the aimed molecule.[44,47] A direct consequence of this mechanism is that the major part of the fragments originates from the aimed molecule, and very few of them from the surrounding molecules. This implication is demonstrated by the distribution of distances between the fragment precursors and the impact points (C_2H_2 in Figure 4b and C_6H_5 in Figure 4c). Although the number of fragments sputtered from molecules that are not aimed by the PP is slightly larger at 5 keV, all the fragment distributions are narrow with a sharp maximum in the 0−5 Å region, regardless of the PP energy. Therefore, in contrast to entire molecules, the yield of fragments appears strongly limited by the number of candidates available in the single, aimed molecule. In our opinion, this is the major cause of the saturation of the fragment yield observed for overlayers on metal surfaces.

(b) High Sputtering Yield Trajectories. Once the global evolution of the yields of ejected species has been established, it is useful for the definition of high sputtering events to classify the yields as a function of the type of event and to examine the probability of each type of event, i.e., the corresponding fraction of trajectories. Because we are mostly interested in the ejection of the top layer organic molecules, a preliminary classification of the sputtering events can be easily made using the number of ejected molecules per event. The probability of events leading to the emission of one to eight molecules is displayed in Figure 5a for the four considered PP energies. The corresponding yields are shown in Figure 5b. Below 1 keV, events that do not eject any molecule strongly predominate, and trajectories where more than one molecule is emitted are rare. The emission of more than two molecules is never observed. Above 1 keV, the probability to eject zero molecules drops below 0.5 and, therefore, scenarios in which one or several molecules are sputtered significantly increase. Nevertheless, the probability to eject more than two molecules is still only ∼4% at 1.5 keV. The distribution broadens significantly at 5 keV and this probability increases to ∼26%. The corresponding yields [event probability X number of ejected molecules per event] provide another perspective on the dramatic change accompanying the PP energy increase. In particular, the distributions of Figure 5b show that the molecule yield increase between 1.5 and 5 keV is mostly caused by the appearance of trajectories where three or more molecules eject. Therefore, if the ejection of three molecules or more is chosen as the condition for high sputtering yield, the onset of high yield events takes place between 1.5 and 5 keV for this system. In section 3.2 and 3.3, the mechanistic views of various sputtering events and the analysis of the kinetic energy distributions will confirm that this "threshold" for high sputtering yield is a reasonable choice and that it has a physical basis.

(c) High Action Trajectories. In the terminology used in the literature, high sputtering yield and high action events are not clearly distinct because, intuitively, a high emission yield is necessarily thought to arise from high action in the sample. In this paragraph, we explore the relationship between high action and high sputtering yield in order to elucidate different emission scenarios. To define high action in the substrate in a similar way as is done for high sputtering yield, we need a reliable parameter measuring action in the substrate. Among other possibilities, the displacement of the silver atoms during the evolution of the trajectories appears to be a good indicator of the action unfolding in the crystal. Therefore, to measure action in the silver crystal, we count the number of silver atoms that are displaced by 10 Å or more in the course of the cascade propagation. From a microscopic viewpoint, these atoms move at least three lattice positions away from their site of origin.

The relationships of the yield of molecules, silver atoms and total sputtered mass with the number of atoms displaced by at least 10 Å are plotted in Figure 6a−c, respectively, for a subset of 150 trajectories at 5 keV. In Figure 6a, deprotonated molecules and silver−molecule aggregates are considered as ejected molecules and counted as yield. The three frames of Figure 6 show that there is indeed a correlation between yield and displacement in the silver crystal. The best regressions between the different sets of data are indicated by dashed lines in Figure 6. The correlation is far from perfect and the dispersion among the data is large. Therefore, besides low action/low yield and high action/high yield trajectories, there are two other marginal categories of events in which the yields and displacements appear uncorrelated (or even anticorrelated). They can

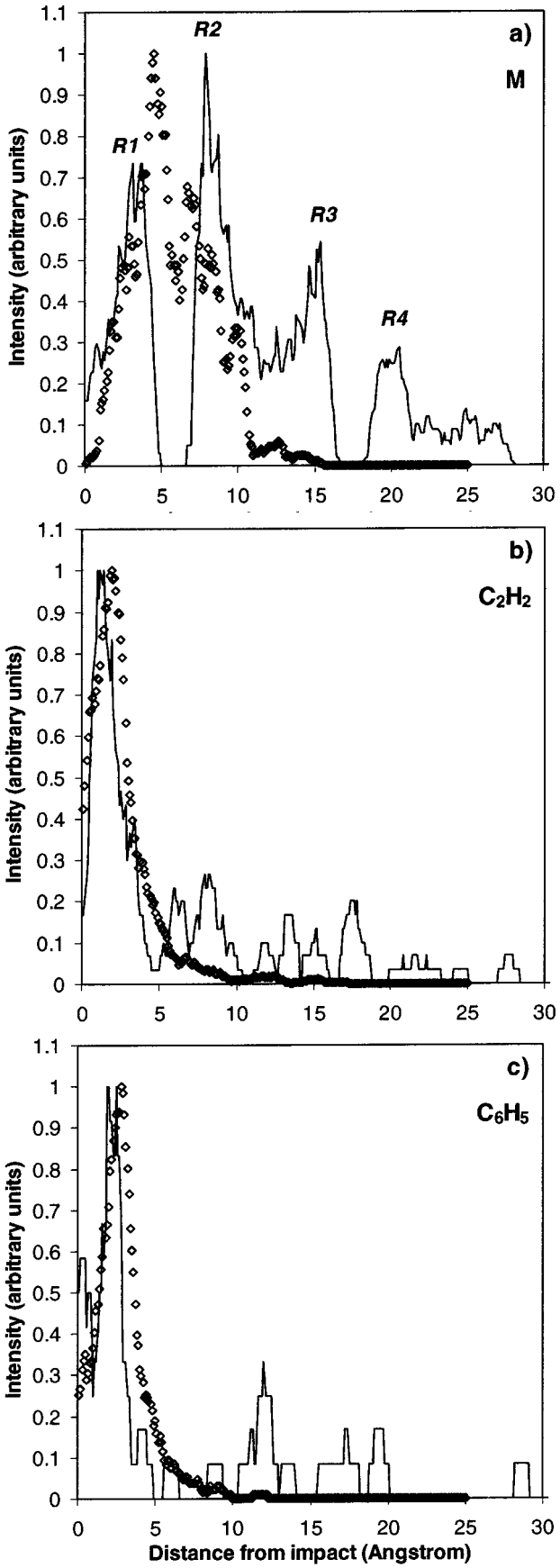

Figure 4. Yield distributions of sputtered species as a function of the distance between their center of mass and the impact point of the primary Ar atom on the surface: (a) entire PS molecule; (b) C_2H_2; (c) C_6H_5. Distributions related to 500 eV and 5 keV Ar bombardment are represented by open diamonds and full lines, respectively. Labels on the peaks indicate which molecules contribute to the corresponding peak, in reference to the labeling used in Figure 1.

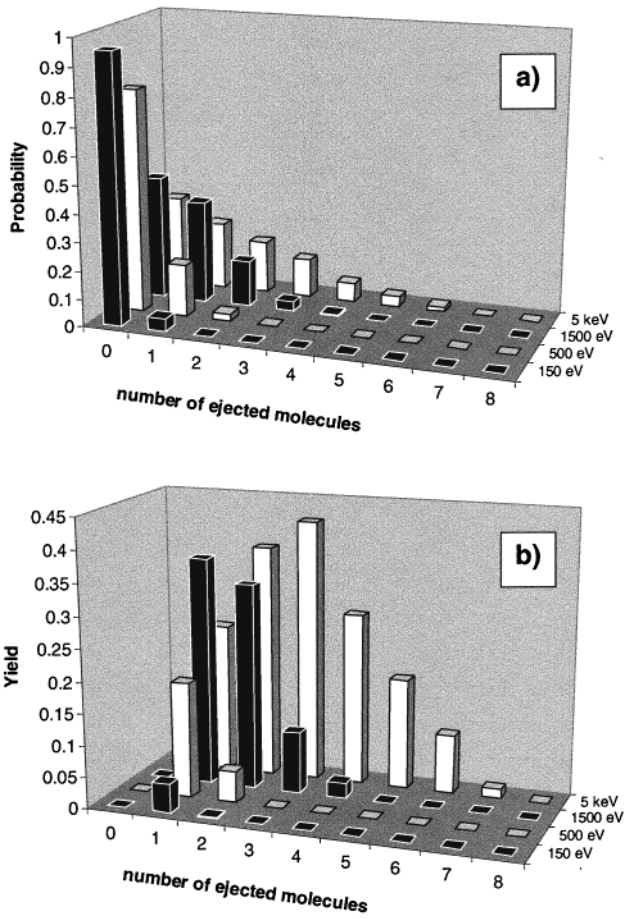

Figure 5. (a) Probability distribution of intact molecule ejection for different primary particle energies. (b) Associated yield distribution [event probability X yield per event].

be referred to as low action/high yield events and high action/low yield events. To go further in this analysis, it is helpful to define a frontier between high action and low action. In Figure 6a, a useful value is provided by the intersection between the regression line and the threshold for high yield events. This value is close to 750 displaced atoms, which roughly corresponds, in volume, to a cube whose sides are one-third of the sides of the silver crystal (one-ninth of the total volume). This definition of high action is arbitrary but it does illuminate classes of motion in the substrate. Consistently, our definition also provides an estimate of high sputtering yield in terms of number of sputtered silver atoms (Figure 6b) and total sputtered mass (Figure 6c). In this respect, trajectories are classified "high yield" if they lead to the sputtering of more than seven silver atoms or a total mass of 2500 amu. With the above definitions, the three plots of Figure 6 are divided in four quadrants numbered I to IV in a clockwise fashion. Quadrant I corresponds to low action/low yield events, quadrant II to low action/high yield events, quadrant III to high action/high yield events and quadrant IV to high action/low yield events. Each quadrant includes a similar fraction of the trajectories across the three plots [quadrant I, ~60%; quadrant II, ~10%; quadrant III, ~25%; quadrant IV, ~5%]. It is interesting to note that, according to our definitions, one-quarter of the trajectories at 5 keV induce high action and high sputtering yields of PS molecules and Ag atoms. Figure 6a provides us with a useful map to pick up interesting trajectories and to identify different mechanistic scenarios, which is the next step of our analysis. The representative trajectories that are described in detail in the following section are identified by capital letters in Figure 6a. Their main characteristics are

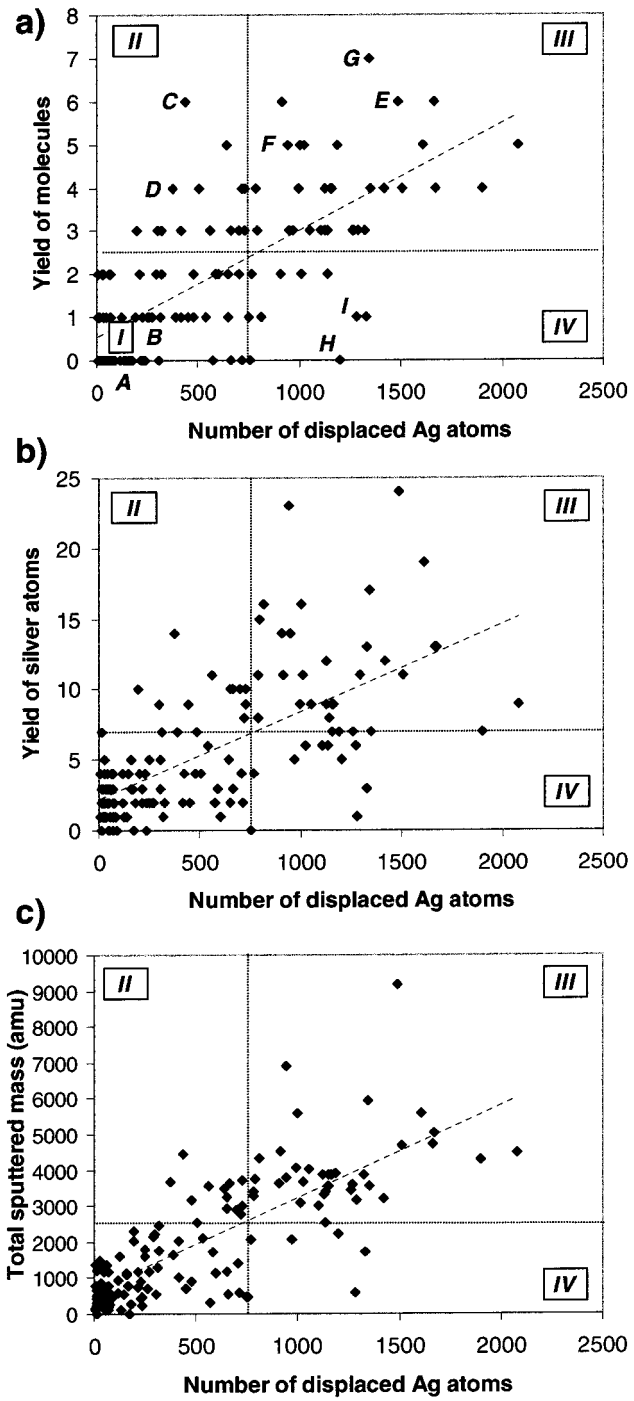

Figure 6. Scatter plots correlating (a) the yield of sputtered molecules, (b) the yield of silver atoms, and (c) the total sputtered mass with the number of silver atoms displaced by 10 Å or more for a subset of 150 trajectories at 5 keV. The four quadrants described in the text are indicated by Roman numbers. The trajectories analyzed in the discussion are labeled with capital letters in frame a. The best linear regressions through the data are indicated by oblique dashed lines in the three frames. The horizontal and vertical dashed lines refer to the definition of high sputtering yield and high action events. See text for details.

summarized in Table 2. Snapshots of the MD simulation corresponding to trajectory E were displayed as an introductory example in Figure 2. In the next section, this trajectory and the other selected examples will be analyzed at length.

3.2. Microscopic View of the Different Event Types. *(a) Collision Trees: Genesis of Action.* To carry out a comprehensive analysis of the various emission scenarios, we examine a representative subset of the 5 keV trajectories in detail. Our

TABLE 2: Major Characteristics of a Small Subset of Trajectories Representing the Four Scenarios of Action/Sputtering

trajectory	fig.	quadrant (see Figure 6)	no. of displaced atoms	no. of sputtered Ag atoms[a] ([b])	no. of ejected PS molecules[c]	energy leaving the crystal
A	7	I	54	1 (0)	0	3943
B	7	I	71	1 (0)	1	3531
C	8	II	439	9 (4)	6	2379
D	8	II	373	14 (2)	4	2916
E	2, 11	III	1487	24 (24)[d]	6	405
F	9	III	941	23 (2)	5	1365
G	9	III	1341	17 (3)	7	975
H	10	IV	1200	5 (7)	0	1308
I	10	IV	1280	1 (0)	1	3162

[a] Ejected as single silver atoms. [b] Ejected as clusters. [c] Including deprotonated molecules and molecule−silver aggregates. [d] 8 dimers, 1 trimer, and 1 pentamer.

major tools for unraveling the mechanistic details of the trajectories are the movies provided by the MD simulations. Indeed, the careful analysis of the sequence of snapshots of a trajectory as a function of time provides the microscopic view of the action that is definitely inaccessible to experiments. To get insights into the high energy part of the cascade which constitutes the genesis of any later action and sputtering, however, another kind of representation is more useful. In the same vein as the "lean-on" trees developed by Harrison, we build up a plot which summarizes the action occurring in the crystal over the first 100 fs of the trajectory. Such a collision tree has been introduced in Figure 2d and others are described in the following discussion (Figures 7−10). The essential strength of this representation is to show the successive positions of the moving atoms as a function of time in a single plot. Using adequate energy filters to decide whether an atom will be shown or not, we can select the moment of the cascades in which we are particularly interested. To make the genesis of action and sputtering clear, a relatively high energy threshold is chosen. In Figure 2d and Figures 7−10, recoil atoms are shown if the collision by which they are set in motion transfers to them more than 100 eV. For the sake of clarity in the figures, it was also decided to "turn off" the atoms when their energy falls below 25 eV. In all these collision trees, the different atoms are distinguished using different colors, and in particular, the incident Ar atom is bright yellow. The main focus of these plots is to define the flow of large amounts of energy in the collision cascade.

Typical collision trees of trajectories corresponding to low action and low sputtering yield [quadrant I in Figure 6] are shown in Figure 7. Additional details concerning the trajectories analyzed in Figures 7−10 can be found in Table 2. There are a few characteristic features which can be deduced from these collision trees and apply to this type of trajectories in general. First, the PP traverses the whole crystal without being strongly deflected by the collisions occurring in the sample. Consequently, it leaves the bottom of the crystal with a significant amount of energy (usually more than 3 keV). Even if the simulation cell were larger, such a deep implantation of the PP energy in the crystal would be unable to induce any more sputtering. On the other hand, it might create important damage (or action) deeper in the sample. The number of high energy recoil atoms in such events is low and insufficient to redirect a significant part of the dissipated energy toward the surface. Finally, the second collision tree in Figure 7 indicates that subcascades in the silver crystal can be induced by carbon atoms initially belonging to the polystyrene molecules, such as the

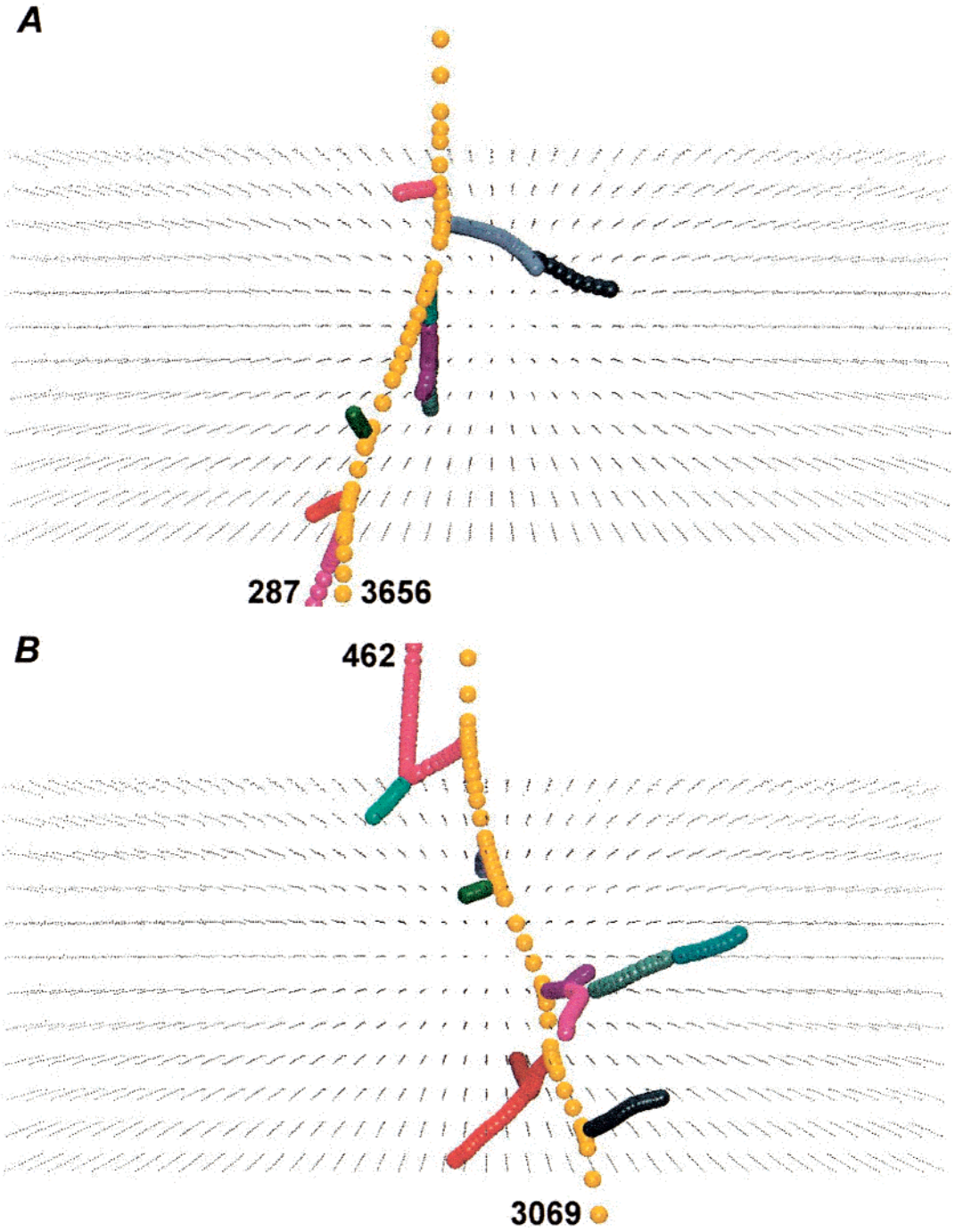

Figure 7. Characteristic collision trees of the first 100 fs of the interaction for low action/low yield events (trajectories A and B in Figure 6a; quadrant I). The successive positions of the recoil atoms are indicated by colored spheres provided that they are set in motion with more than 100 eV of energy. They are "turned off" when their energy falls below 25 eV. The numbers on the charts refer to the quantity of energy in electronvolts leaving the crystal with the corresponding atoms.

pink atom reflected by the top silver layer in trajectory B (see also trajectory H).

It is particularly intriguing that a number of trajectories induce high sputtering yields with a limited action in the sample [quadrant II in Figure 6]. Two of these events are illustrated in Figure 8. Again, a significant fraction of the PP energy leaves the crystal, mostly through the bottom in case C and with the backscattered PP in case D. In contrast with the first scenario, these examples show that most of the energetic recoils are created in the top silver layers, leading quickly to an efficient reversal of the momentum direction toward the surface. Although the action is limited, according to our definition, it is confined in the surface of the sample, therefore inducing high sputtering yields. From the viewpoint of the SIMS analysis, it is probably the more efficient mechanism, since it generates large ejection yields associated with low damage.

An example of high action and high yield event [quadrant III in Figure 6] has been shown in Figure 2. This trajectory is labeled E in Table 2 and the associated collision tree is displayed in Figure 2d. In this trajectory, the energy of the primary particle is nearly entirely dissipated among the atoms of the silver crystal. After a violent collision with a first layer silver atom, the PP channels momentarily along the silver planes and undergoes multiple high energy collisions in the top four layers of the crystal. As described in section 3.1, the final result is the massive ejection of silver atoms, clusters and PS molecules.

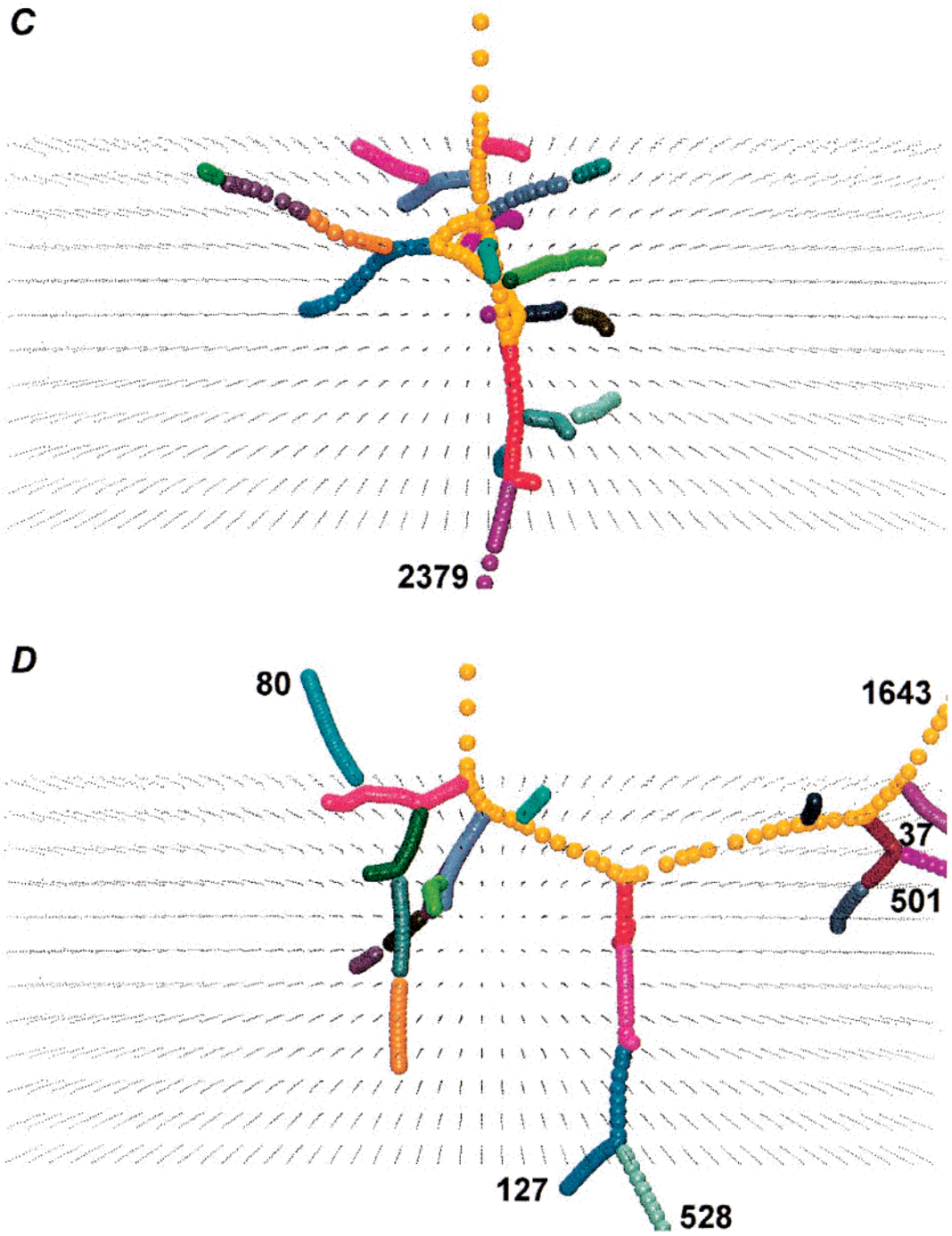

Figure 8. Characteristic collision trees for low action/high yield events (trajectories C and D in Figure 6a; quadrant II).

Two other examples of high action/high yield trajectories (F, G) are shown in Figure 9. In trajectory F, the high action is mostly developing in the upper part of the crystal because of a very energetic collision of the Ar atom with a top layer silver atom. Afterward, the PP is successively reflected by several silver atoms in the top three layers, where it distributes all of its energy. In trajectory G, the action extends within the depth of the sample. There are common features in the E, F and G trajectories. First, the Ar atom is trapped in the crystal and most of its energy is quickly dissipated through a number of high energy collisions with Ag atoms. Second, these energetic silver atoms evolving simultaneously in a limited space lead to subcascade overlapping and high action. The large quantity of energy distributed locally induces a propensity of the crystal to expand from its free surfaces toward the vacuum, as exemplified in Figure 2c.

The last category of trajectories corresponds to quadrant IV in Figure 6. Two collision trees of such events (H, I) are shown in Figure 10. In both cases, the PP goes through the top layers of the crystal without strongly interacting, and its energy is mostly dissipated deeper in the sample where high action is generated. The momentum is not efficiently redirected toward the surface and a low sputtering yield ensues.

The above examples illustrate quite clearly the four major scenarios observed in the MD simulations. With our analysis of the collision trees, the genesis of these events can be explained. In addition, the very last stage of the sputtering process is well described by snapshots of the trajectories such

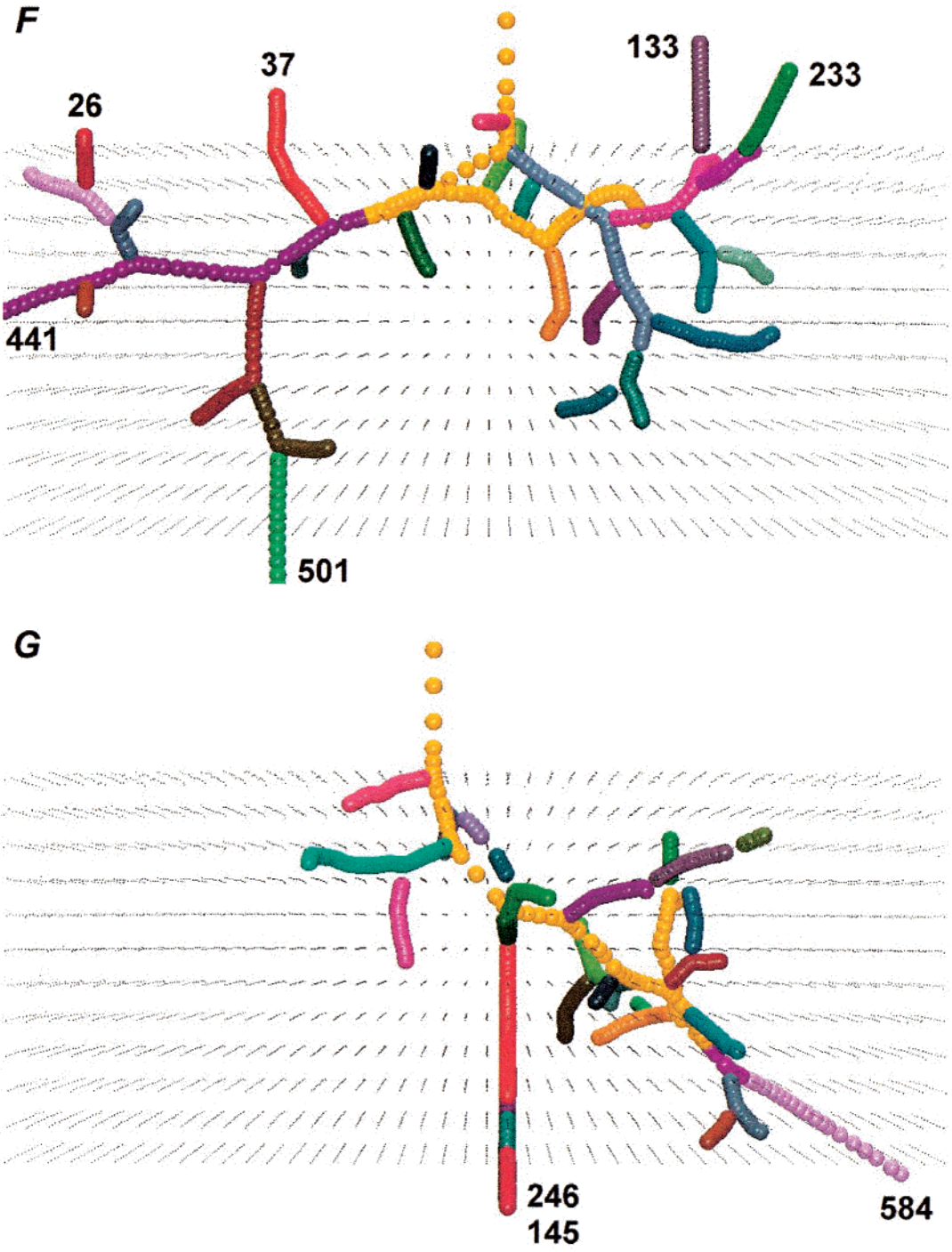

Figure 9. Characteristic collision trees for high action/high yield events (trajectories F and G in Figure 6a; quadrant III).

as shown in Figure 2a−c. Nevertheless, the intermediate stages of the cascade development, when the energy is transferred from the subset of fast atoms to a larger number of much slower atoms, are not fully elucidated. In the next subsection, complementary information concerning these stages is provided by snapshots of the simulation showing the energy of the atoms in the cascade.

(b) Energy Transfer and Cooling of Energetic Recoil Atoms. The link between the early development of energetic cascades (Figure 2d) and the massive sputtering of atoms and molecules (Figure 2c) in the latest times of the interaction with the PP is not obvious. To clarify this link, snapshots showing the time evolution of the Ag atom energies up to ~200 fs are presented in Figure 11 for trajectory E. The energies of the atoms are indicated by their size and hue. The chosen size/hue code underlines the low energy part of the cascades. Indeed, the largest spheres correspond to atoms with a kinetic energy of 5 eV or more. Below this upper size limit, the radius of the spheres is directly proportional to their energy. Small dark blue to large turquoise spheres refer to downward moving Ag atoms whereas small red to large yellow spheres correspond to atoms with an upward momentum.

At 26 fs (frame a), the energy is still contained in a small set of energetic atoms, as expected from the collision tree (Figure 2d). The momentum is mostly directed downward, but it begins to be reflected toward the surface through a few upward moving atoms (yellow spheres). Between 58 and 108 fs, the momentum is gradually transferred to a large fraction of the atoms

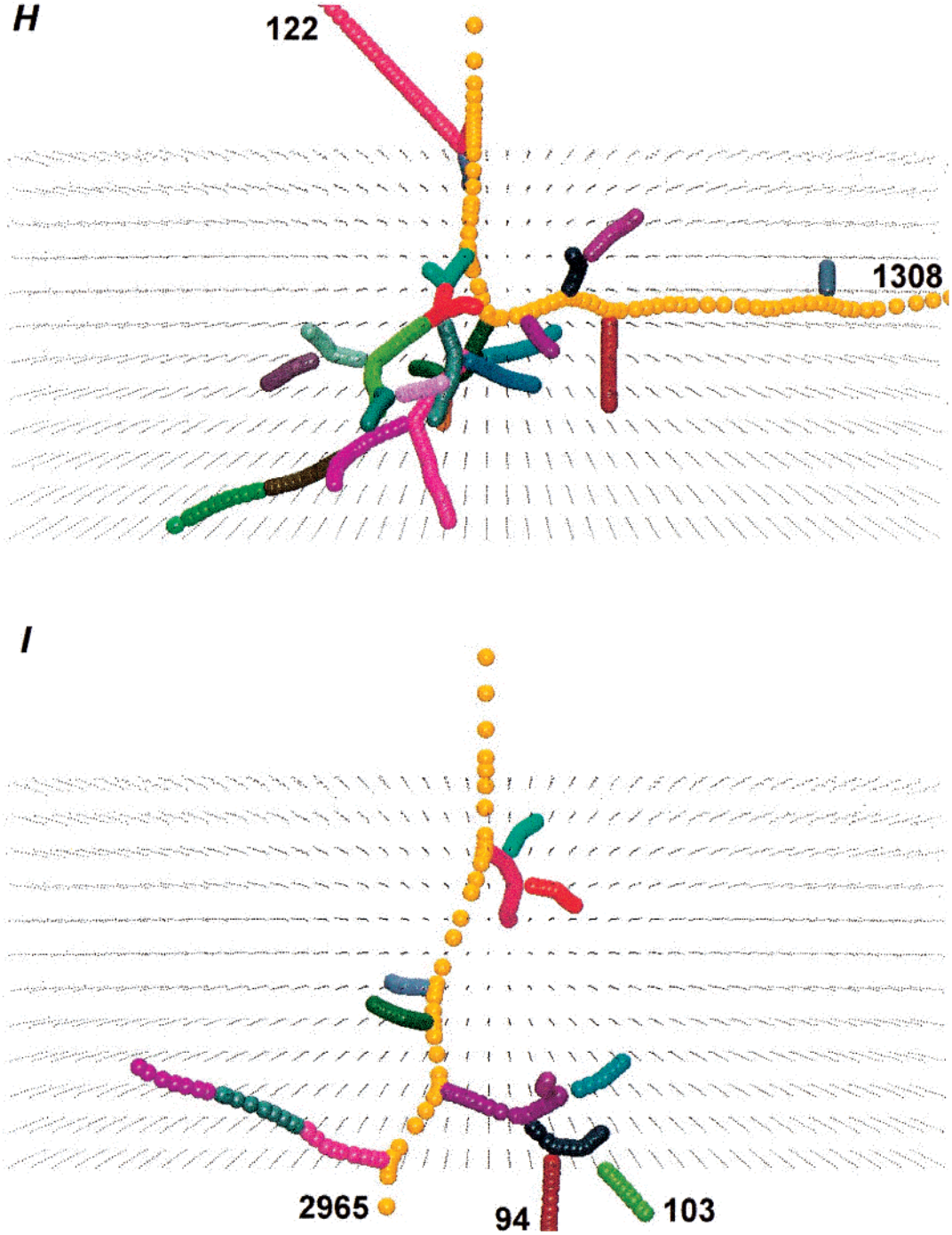

Figure 10. Characteristic collision trees for high action/low yield events (trajectories H and I in Figure 6a; quadrant IV).

surrounding the tracks of the fast recoils (frames b and c). After 192 fs, the excited volume still expands and slowly cools (frame d). Many low energy atoms (<10 eV) are leaving the surface. The chosen color code emphasizes a very interesting feature of the trajectory, which is generally observed in high action events. From the beginning, upward and downward moving atoms are clearly grouped in two separate regions. The downward momentum region propagates toward the bottom of the crystal, through the collective motion of many silver atoms. Likewise, an upward directed collective motion pushes a large number of first and second layer Ag atoms from the crystal into the vacuum. In that sense, high ejection events evoke the concepts of spike or collective motion as described in the shock wave[25] and pressure pulse[30] models. In parallel, the collision trees clearly show the separated energetic subcascades whose subsequent overlapping eventually generates the high action.

3.3. Influence of the High Sputtering Yield Events on the Properties of Sputtered Molecules. *(a) Kinetic Energy Distributions.* In addition to high ejection yields, a signature of the high sputtering yield events can be found in the kinetic energy distributions (KED) of the emitted PS molecules. In Figure 12, the KED of PS molecules sputtered by 500 eV Ar atoms is shown along with two KEDs obtained at 5 keV. The 5 keV KEDs are resolved as a function of the type of event, i.e., low sputtering yield (less than three molecules) and high sputtering yield (three molecules or more). The similarity between the 500 eV and the 5 keV low sputtering yield distributions is striking. It shows that events which eject less

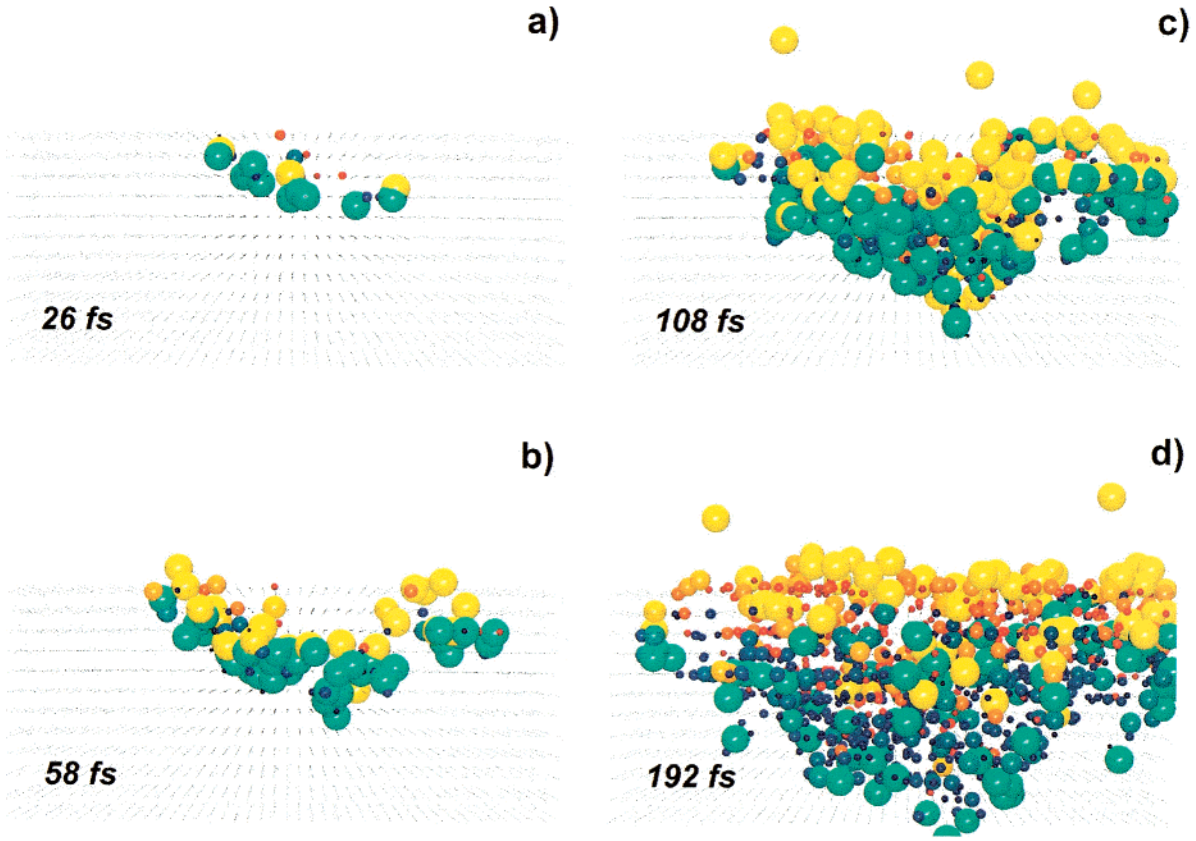

Figure 11. Picture of the kinetic energy of the Ag atoms at different times in the development of a high yield event (trajectory E): (a) 26 fs; (b) 58 fs; (c) 108 fs; (d) 192 fs. Ag atoms moving upward are depicted by red to yellow spheres and Ag atoms moving downward by blue to turquoise spheres. The radius of the spheres is directly proportional to the energy of the atoms up to 5 eV. The largest radius corresponds to atoms with 5 eV or more energy.

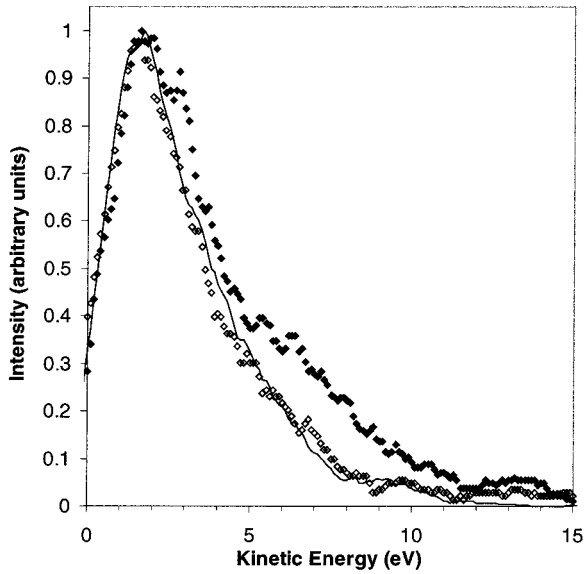

Figure 12. Kinetic energy distributions of intact PS tetramers sputtered by 500 eV and 5 keV Ar atoms. The full line refers to 500 eV and the diamonds to 5 keV Ar bombardment. The 5 keV distributions are resolved as a function of the type of trajectory. High yield events are represented by black diamonds and low yield events by open diamonds.

than three molecules induce the same KEDs, whatever the primary particle energy (500 eV versus 5 keV). In contrast, the 5 keV high sputtering yield distribution is broader and exhibits a more pronounced high energy tail. Figure 12 shows the KEDs of stable molecules, i.e., molecules whose internal energy is lower than the calculated threshold for dissociation (see ref 47 for discussion). Therefore, it is clear that high yield events can give rise to molecules with higher kinetic energies that will reach the detector. This particularity is probably due to the more correlated momentum of the Ag atoms inducing their ejection.

(b) Ejection of Large Organic Molecules. In section 3.1, it has been shown that high action and high yield events are not exceptions under 5 keV Ar atom bombardment. They are observed with 25% of the trajectories according to our definition. Oftentimes, the number and total mass of ejected species is well beyond two thousand daltons. Interestingly, the highest ejected mass observed in our simulations is close to 10 kDa, i.e., the upper mass limit of ejected species in SIMS. Up to 7−8 PS tetramers can be ejected by a single 5 keV Ar atom. In contrast, sub-kiloelectronvolt particle bombardment is unable to induce similar events. In our opinion, such high yield trajectories might explain the emission of molecules of several kilodaltons in SIMS. Indeed, it is reasonable to imagine that the correlated upward motion depicted in Figure 2 might eject organic molecules that are much larger than PS tetramers.

To check this hypothesis, we devised a slightly different sample using the same silver crystal. A top view of the new sample is shown in Figure 13a. Instead of PS tetramers, two PS *hexadecamers* (16 repeat units) are relaxed on the silver surface. The mass of the tritiated PS hexadecamer is ∼2 kDa (1998 Da) and its binding energy to the silver surface is ∼7.2 eV, i.e., three times that of a PS tetramer. To make sure that the first high energy stages of the collision cascade unfold in the same manner as is observed in our previous simulations for a given aiming point, it keeps the PS tetramer belonging to the bombarded area in the center of the sample. The trajectory described in Figure 13 (E′) corresponds to the same aiming point

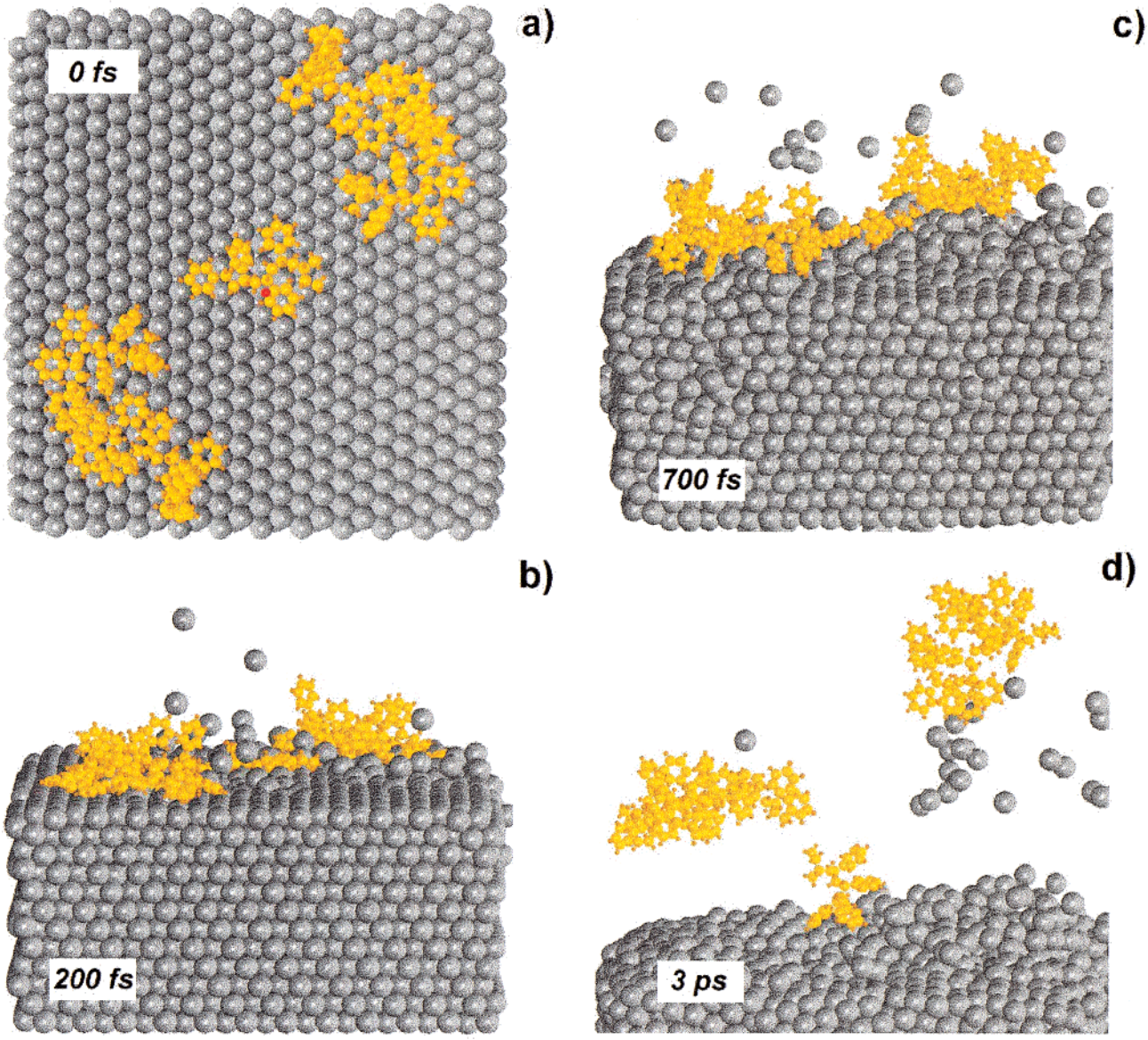

Figure 13. Emission of two PS hexadecamers (1998 Da) induced by a 5 keV Ar atom, with the same aiming point as trajectory E: (a) top view of the sample at 0 fs; (b−d) side views at 200 fs (b), 700 fs (c), and 3000 fs (d).

as trajectory E, but with the new sample. The analysis of trajectory E′ indicates that the early development of the collision cascade in the silver crystal is indeed very similar to that observed in trajectory E (Figure 2). At 200 fs, a few single Ag atoms are emitted and a collective motion including several tens of Ag atoms begins under the top right PS oligomers. After 700 fs, a large protrusion is created by the correlated motion of these atoms, pushing the PS oligomer upward. In the same time, the bottom left PS molecule is smoothly lifted up, although the action in that part of the top silver layer is less apparent. Many silver atoms and clusters are emitted, as was the case in trajectory E. After a few picoseconds, the two PS hexadecamers are evolving in the vacuum, out of influence of the silver surface. The molecule on the right is accompanied by a large silver cluster which will probably decay into smaller pieces due to its internal energy excess. In contrast, the two PS molecules should not decompose on the time scale of SIMS analysis (∼150 μs) according to the RRK theory (see the stability check protocol in ref 47). Our simulations indicate that the ejection of PS hexadecamers in high action events such as trajectory E′ is not exceptional. For larger organic molecules, we believe that the intramolecular van der Waals forces, not taken into account in the above simulations, might play a significant role in the ejection process. Therefore, it would be precarious to run similar simulations with heavier molecules without including these long-range forces.

The action depicted in Figure 13 demonstrates that trajectories which satisfy our definition of high action and high sputtering yield (section 3.1) are also able to induce the ejection of larger molecules. For this reason, it appears quite clearly that the collective motions that are the key to high sputtering yield of intermediate size molecules such as PS tetramers also constitute the most efficient mechanism for the emission of much heavier organic molecules. Finally, the gradual increase of the influence of the high yield-type events with increasing molecule size is further supported by experimental studies of the ejection of PS oligomers in the range 500−3000 Da, whose KEDs broaden significantly with mass.[64]

An extensive study of the influence of the different physical parameters on the proportion and amplitude of high yield events would be useful in order to extend the accessible mass range in SIMS. The optimization of the primary beam parameters, e.g.

primary particle mass, energy and nature (polyatomic projectiles), might lead to the desired improvement. The investigation of the relationship between the primary beam and the target characteristics,[43] e.g., metal substrate versus organic matrix, might even be more crucial to obtain a significant enhancement of the performance in SIMS. For instance, the use of carbon clusters in conjunction with bulk organic samples provides impressive results, as demonstrated by Gillen et al.[65] It is our belief that such yield enhancements are related to dramatic events bearing some resemblance to those described in this paper.

4. Conclusion

Molecular dynamics simulations indicate that the massive ejection of substrate atoms, clusters, and molecules can be induced by kiloelectronvolt particle bombardment of organic overlayers on metals. The proportion of high yield events strongly depends on the primary particle energy. For example, they are absent in the sub-kiloelectronvolt regime, become apparent at 1.5 keV and become really significant at 5 keV. Interestingly, high yield events increase the yield of intact organic molecules, and not the yield of fragments.

The collision trees and the snapshots of the MD simulations provide insights into the microscopic interactions that generate high yield events. In general, these events are caused by the dissipation of most of the primary particle energy in the top few layers of the metal substrate. The momentum is first transferred to a small subset of atoms through high energy collisions, then distributed to the whole surrounding volume. The high energy density induced by the subcascades overlapping leads to the simultaneous motion of the major part of the atoms located in the excited volume. The expansion and cooling of the excited region finally induces the ejection of large quantities of material. Although the size of the excited volume is quite limited in comparison with other types of interactions, e.g., laser ablation or megaelectronvolt particle bombardment, the observed phenomenon bears resemblance with the concepts used to describe those interactions. In particular, the propagation of the momentum simultaneously toward the bottom and to the top of the sample through a large number of particles, shown by the snapshots of the MD simulations, can be described in terms of collective motion of atoms, as is the case for laser ablation. These collective motions are efficient to desorb large molecules with a mass of 2 kDa.

We believe that the systematic investigation of the parameters influencing high sputtering yield events constitutes the best means to improve the performance of static SIMS analysis with respect to sputtering yield and accessible mass range. The combination of MD simulations and carefully designed SIMS experiments appears to be the method of choice to reach this goal. Therefore, we plan to extend this method to different samples, e.g. larger molecules, molecular solids, and to different primary beam characteristics in the future.

Acknowledgment. The authors thank Kristin Krantzman for helpful discussion and advice. The financial support of the National Science Foundation through the Chemistry Division, the CRIF program and the MRI program are gratefully acknowledged by A.D. and B.J.G. Additional computational resources were provided in part by the IBM Selected University Resource Program and the Center for Academic Computing of Penn State University. We are also indebted to the Center for Academic Computing staff for helping us use the IBM SP computer and for the development of a new graphics software for animation and presentation.

References and Notes

(1) Barber, M.; Bordoli, R. S.; Sedgwick, R. D.; Tyler, A. N. *J. Chem. Soc., Chem. Commun.* **1981**, 325.
(2) Benninghoven, A.; Sichtermann, W. K. *Anal. Chem.* **1978**, *50*, 1180.
(3) Gusev, A. I.; Choy, B. K.; Hercules, D. M. *J. Mass Spectrom.* **1998**, *33*, 480.
(4) Hagenhoff, B. In *The Static SIMS Library*; Vickerman, J. C., Briggs, D., Henderson, A., Eds; SurfaceSpectra: Manchester, 1997; p 39.
(5) Linton, R. W.; Mawn, M. P.; Belu, A. M.; DeSimone, J. M.; Hunt, M. O., Jr.; Menceloglu, Y. Z.; Cramer, H. G. *Surf. Interface Anal.* **1993**, *20*, 991.
(6) Wu, K. J.; Odom, R. W. *Anal. Chem.* **1996**, *68*, 873.
(7) Hillenkamp, F.; Karas, M.; Beavis R. C.; Chait, B. T. *Anal. Chem.* **1991**, *63*, 1193A.
(8) Lorenz, S. A.; Maziarz, E. P.; Wood, T. D. *Appl. Spectrosc.* **1999**, *53*, 18A.
(9) Berkenkamp, S.; Menzel, C.; Karas, M.; Hillenkamp, F. *Rapid Commun. Mass Spectrom.* **1997**, *11*, 1399.
(10) Menzel, C.; Berkenkamp, S.; Hillenkamp, F. *Rapid Commun. Mass Spectrom.* **1999**, *13*, 26.
(11) Chen, R.; Cheng, X.; Mitchell, D. W.; Hofstadler, S. A.; Wu, Q. *Anal. Chem.* **1995**, *67*, 1159.
(12) Benninghoven, A.; Rüdenauer, F. G.; Werner, H. W. *Secondary Ion Mass Spectrometry*; Wiley: New York, 1987; p 699.
(13) Odom, R. W. In *Microscopic and Spectroscopic Imaging of the Chemical State*; Morris, M. D., Ed; Marcel Dekker: New York, 1993; p 345.
(14) *Secondary Ion Mass Spectrometry, SIMS XI Proceedings*; Gillen, G., Lareau, R., Bennett, J., Stevie, F., Eds.; Wiley: New York, 1998.
(15) Zhigilei, L. V.; Kodali, P. B. S.; Garrison, B. J. *J. Phys. Chem. B* **1998**, *102*, 2845.
(16) Sigmund, P. In *Sputtering by Particle Bombardment I*; Behrisch, R., Ed;. Springer: Berlin, 1981; p 9.
(17) Sigmund, P.; Claussen, C. *J. Appl. Phys.* **1981**, *52*, 990.
(18) Miotello, A.; Kelly, R. *Nucl. Instrum. Methods B* **1997**, *122*, 458.
(19) Urbassek, H. M. *Nucl. Instrum. Methods B* **1997**, *122*, 427.
(20) Harrison, D. E., Jr. *Crit. Rev. Sol. State Mater. Sci.* **1988**, *14*, S1.
(21) Shapiro, M. H.; Tombrello, T. A. *Nucl. Instrum. Methods B* **1999**, *152*, 221.
(22) Andersen, H. H.; Brunelle, A.; Della-Negra, S.; Depauw, J.; Jacquet, D.; Le Beyec, Y. *Phys. Rev. Lett.* **1998**, *80*, 5433.
(23) David, D. E.; Magnera, Th. F.; Tian, R.; Stulik, D.; Michl, J. *Nucl. Instrum. Methods B* **1986**, *14*, 378.
(24) Urbassek, H. M.; Michl, J. *Nucl. Instrum. Methods B* **1987**, *22*, 480.
(25) Carter, G. *Radiat. Eff. Lett.* **1979**, *43*, 193.
(26) Carter, G. *Nucl. Instrum. Methods* **1983**, *209/210*,1.
(27) Bitenski, I. S.; Parilis, E. S. *Nucl. Instrum. Methods B* **1987**, *21*, 26.
(28) Bitenski, I. S. *Nucl. Instrum. Methods B* **1993**, *83*, 110.
(29) Mahoney, J. F.; Perel, J.; Lee, T. D.; Martino, P. A.; Williams, P. *J. Am. Soc. Mass Spectrom.* **1992**, *3*, 311.
(30) Johnson, R. E.; Sundqvist, B. U. R.; Hedin, A.; Fenyo, D. *Phys. Rev. B* **1989**, *40*, 49.
(31) Kitazoe, Y.; Yamamura, Y. *Rad. Eff. Lett.* **1980**, *50*, 39.
(32) Yamamura, Y. *Nucl. Instrum. Methods* **1982**, *194*,515.
(33) Webb, R. P.; Harrison, D. E., Jr *Appl. Phys. Lett.* **1981**, *39*, 311.
(34) Wong, S. S.; Rollgen, F. W. *Nucl. Instrum. Methods B* **1986**, *14*, 436.
(35) Sundqvist, B. U. R. *Nucl. Instrum. Methods B* **1990**, *48*, 517.
(36) Waldeer, K. T.; Urbassek, H. M. *Nucl. Instrum. Methods B* **1993**, *73*, 14.
(37) Webb, R. P.; Harrison, D. E. *Nucl. Instrum. Methods B* **1984**, *2*, 660.
(38) Ghaly, M.; Averback, R. S. *Phys. Rev. Lett.* **1994**, *72*, 364.
(39) Betz, G.; Husinsky, W. *Nucl. Instrum. Methods B* **1995**, *102*, 281.
(40) Husinsky, W.; Betz, G. *Thin Solid Films* **1996**, *272*, 289.
(41) Betz, G.; Dandachi, C.; Husinsky, W. *Izv. Akad. Nauk: Ser. Fiz.* **1998**, *62*, 690.
(42) Webb, R. P.; Harrison, D. E. *Phys. Rev. Lett.* **1983**, *50*, 1478.
(43) Townes, J. A.; White, A. K.; Wiggins, E. N.; Krantzman, K. D.; Garrison, B. J.; Winograd, N. *J. Phys. Chem. B* **1999**, *103*, 4587.
(44) Nguyen, T. C.; Ward, D. W.; Townes, J. W.; White, A. K.; Krantzman, K. D. *J. Phys. Chem.*, in press.
(45) Beardmore, K.; Smith, R. *Nucl. Instrum. Methods B* **1995**, *102*, 223.
(46) Beardmore, K.; Smith, R. Computer animations available online at http://lboro.ac.uk/departments/ma/research/molecular/index.html.

(47) Delcorte, A.; Vanden Eynde, X.; Bertrand, P.; Vickerman, J. C.; Garrison, B. J. *J. Phys. Chem. B* **2000**, *104*, 2673.

(48) Garrison, B. J.; Winograd, N.; Harrison, D. E., Jr. *J. Chem. Phys.* **1978**, *69*, 1440.

(49) Winograd, N.; Garrison, B. J. In *Ion Spectroscopies for Surface Analysis*; Czanderna, A. W., Hercules, D. M., Eds.; Plenum Press: New York, 1991; p 45.

(50) Garrison, B. J. *J. Chem. Soc. Rev.* **1992**, *21*, 155.

(51) Bernardo, D. N.; Bhatia, R.; Garrison, B. J. *Comput. Phys. Commun.* **1994**, *80*, 259.

(52) Chatterjee, R.; Postawa, Z.; Winograd, N.; Garrison, B. J. *J. Phys. Chem. B* **1999**, *103*, 151.

(53) Stave, M. S.; Sanders, D. E.; Raeker, T. J.; DePristo, A. E. *J. Chem. Phys.* **1990**, *93*, 4413.

(54) Raeker, T. J.; DePristo, A. E. *Int. Rev. Phys. Chem.* **1991**, *10*, 1.

(55) Kelchner, C. L.; Halstead, D. M.; Perkins, L. S.; Wallace, N. M.; DePristo, A. E. *Surf. Sci.* **1994**, *310*, 425.

(56) Brenner, D. W. *Phys. Rev. B* **1990**, *42*, 9458.

(57) Brenner, D. W.; Harrison, J. A.; White, C. T.; Colton, R. J. *Thin Solid Films* **1991**, *206*, 220.

(58) Taylor, R. S.; Garrison, B. J. *Langmuir* **1995**, *11*, 1220.

(59) Dudde, R.; Frank, K. H.; Koch, E. E. *Surf. Sci.* **1990**, *225*, 267.

(60) Anderson, A. B.; McDevitt, M. R.; Urbach, F. L. *Surf. Sci.* **1984**, *146*, 80.

(61) Harrison, D. E., Jr.; Delaplain, C. B. *J. Appl. Phys.* **1976**, *47*, 2252.

(62) Wucher, A.; Garrison, B. J. *Phys. Rev. B* **1992**, *46*, 4855.

(63) Sanders, D. E.; Prasad, K. B. S.; Burnham, J. S.; Garrison, B. J. *Phys. Rev. B* **1994**, *50*, 5358.

(64) Delcorte, A.; Bertrand, P. *Surf. Sci.* **1998**, *412/413*, 97.

(65) Gillen, G. In *Secondary Ion Mass Spectrometry, SIMS XII Proceedings*; Benninghoven, A., Bertrand, P., Migeon, H.-N., Eds.; Elsevier: Amsterdam, 2000; in press.